Cerebral Cortex August 2014;24:2237–2248
doi:10.1093/cercor/bht085
Advance Access publication March 31, 2013

Motor Cortex Broadly Engages Excitatory and Inhibitory Neurons in Somatosensory Barrel Cortex

Amanda K. Kinnischtzke[1,2], Daniel J. Simons[1,2] and Erika E. Fanselow[1,2]

[1]Center for Neuroscience, University of Pittsburgh, [2]Department of Neurobiology, University of Pittsburgh School of Medicine, Pittsburgh, PA 15261, USA

Address correspondence to Amanda Kinnischtzke, Department of Neurobiology, University of Pittsburgh School of Medicine, E1440 BSTWR, 200 Lothrop St., Pittsburgh, PA 15261, USA. Email: akk31@pitt.edu

Anatomical studies have shown that primary somatosensory (S1) and primary motor (M1) cortices are reciprocally connected. The M1 to S1 projection is thought to represent a modulatory signal that conveys motor-related information to S1. Here, we investigated M1 synaptic inputs to S1 by injecting an AAV virus containing channelrhodopsin-2 and a fluorescent tag into M1. Consistent with previous results, we found labeling of M1 axons within S1 that was most robust in the deep layers and in L1. Labeling was sparse in L4 and was concentrated in the interbarrel septa, largely avoiding barrel centers. In S1, we recorded in vitro from regular-spiking excitatory neurons and fast-spiking and somatostatin-expressing inhibitory interneurons. All 3 cell types had a high probability of receiving direct excitatory M1 input. Both excitatory and inhibitory cells within L4 were the least likely to receive such input from M1. Disynaptic inhibition was observed frequently, indicating that M1 recruits substantial inhibition within S1. Additionally, a subpopulation of L6 regular-spiking excitatory neurons received exceptionally strong M1 input. Overall, our results suggest that activation of M1 evokes within S1 a bombardment of excitatory and inhibitory synaptic activity that could contribute in a layer-specific manner to state-dependent changes in S1.

Keywords: active touch, cortical circuits, interneurons, optogenetics, sensorimotor integration

Introduction

During active touch, sensory and motor-related signals are thought to interact in a fashion that regulates on-going exploration and stimulus discriminability. In the rodent whisker system the motor and somatosensory systems are intricately linked at the level of brainstem, thalamus, and cortex (Kleinfeld et al. 2006), providing multiple mechanisms for sensorimotor integration. At the cortical level, primary motor (M1) and primary somatosensory (S1) cortices are reciprocally connected (White and DeAmicis 1977; Porter and White 1983), with the S1 to M1 connection thought to represent the "forward" pathway, and M1 to S1 to represent the "backward" pathway (Felleman and Van Essen 1991; Cauller et al. 1998). In keeping with this view, recent studies have demonstrated that the synaptic inputs from S1 to M1 are stronger than those from M1 to S1 (Rocco-Donovan et al. 2011). In addition, sensory-evoked activity is first present in S1 and subsequently propagated to M1 (Ferezou et al. 2007).

Functionally, the role of M1 inputs is hypothesized to play a "modulatory" role within S1 by sending a copy of motor-related information that could alter processing of whisking-related sensory information in S1 (Fee et al. 1997; Kleinfeld et al. 2006; Hill et al. 2011; Friedman et al. 2012). Neurons in M1 are active prior to and during whisking (Carvell et al. 1996; Friedman et al. 2006), at which time S1 neurons exhibit smaller responses to whisker deflection (Chapin and Woodward 1982; Fanselow and Nicolelis 1999; Ferezou et al. 2007). In addition, pairs of S1 neurons exhibit a reduction in membrane potential correlation relative to non-whisking states (Poulet and Petersen 2008). The peripheral and/or central origin of many of these state-dependent changes in S1 is unclear; however, given the extensive reciprocal connectivity between M1 and S1, whisking-associated changes in S1 firing could reflect direct M1 to S1 projections.

An understanding of M1–S1 interactions has been hindered by the inability to activate selectively motor cortex inputs to S1. In reciprocally connected neural systems, commonly used techniques involving electrical stimulation may be confounded by inadvertent antidromic activation of cells in the target population via their locally recurrent axons. The recent development of optogenetic tools allows for selective activation of neuronal populations that project to a distant location, permitting investigation of the properties of their synaptic connections. In addition, mapping of connectivity between M1 and S1 has so far focused solely on inputs to excitatory neurons (Petreanu et al. 2009; Mao et al. 2011; Rocco-Donovan et al. 2011). However, inhibitory interneurons can regulate the impact of excitatory inputs between brain areas, such as thalamus to cortex, through feedforward inhibition (Simons and Carvell 1989; Pouille and Scanziani 2001; Swadlow 2003; Gabernet et al. 2005). Inhibitory interneurons comprise a diverse group (Markram et al. 2004; Ascoli et al. 2008), and the effect of inhibition on sensory processing is dependent on the types of inhibitory interneurons involved (Porter et al. 2001; Pouille and Scanziani 2004; Lee et al. 2012; Wilson et al. 2012).

Here, we utilized an optogenetic approach combined with in vitro whole-cell recordings to examine synaptic inputs from M1 onto specific classes of excitatory and inhibitory cells in S1. We focused on 3 identified types of neurons in S1: regular-spiking (RS) pyramidal neurons, fast-spiking (FS) inhibitory interneurons, and somatostatin-expressing (SOM) inhibitory interneurons. We recorded responses in vitro from each of these cell types in S1 evoked by photic activation of M1 terminals expressing channelrhodopsin-2 (ChR2). Our findings indicate a high probability of M1 input to all 3 cell types. The nature of the inputs is laminar and cell-type specific. Results demonstrate that both inhibitory and excitatory neurons are strongly and widely recruited by M1, providing circuit-level mechanisms for the regulation of S1 activity during movement-associated activity in M1.

Methods

All experiments were carried out in compliance with the University of Pittsburgh School of Medicine animal use policies and were approved by the University of Pittsburgh Institutional Animal Care and Use Committee.

Virus injections

Experiments were conducted using a transgenic mouse line that contains GFP in a subset of SOM-expressing GABAergic neurons ("GIN" mice; Oliva et al., 2000). Mice were first anesthetized using isoflurane (1–2%/oxygen), a small craniotomy was performed over primary motor cortex (1.0 mm anterior to and 0.8 mm lateral from bregma), and the adeno-associated virus AAV2/5.CamKIIα.hChR2(H134R)-mCherry.WPRE.SV40 (University of Pennsylvania Vector Core; permission from Dr. Karl Deisseroth) was unilaterally pressure injected into primary motor cortex (M1) using a picospritzer. In a single penetration, we injected the virus separately into both deep and superficial layers of M1 (0.8 and 0.4 mm depth, respectively). A volume of 0.1–0.2 μL was injected at each depth. At the time of injection, the mice were 10–15 postnatal days of age (P10–P15).

Verification of M1-to-S1 labeling

At the outset, we examined the nature of the ChR2 labeling. Injected animals were perfused transcardially using 0.1 M PBS followed by 4% paraformaldehyde. The brain was then placed in 30% sucrose for 48–72 h. Next, the brain was frozen and sectioned in either the coronal or tangential plane at 40 μm using a cryostat.

Initial experiments were done using the AAV2/1.CAG.hChR2(H134R)-mCherry.WPRE.SV40 viral vector. When the tissue was examined, we consistently observed ChR2-mCherry labeled cells within S1, suggesting a small percentage of neurons was retrogradely transporting the virus from M1, the injection site, back to S1 (data not shown). Because we wished to examine only M1 inputs to S1 and not possible recurrent collaterals of retrogradely labeled S1 cells, we decided to use AAV2/5.CamKIIα.hChR2(H134R)-mCherry.WPRE.SV40 for all of our experiments, which we thought may result in little or no retrograde transport while still producing strong ChR2-expression in M1 neurons. To confirm this, in a subset of animals injected with this viral vector, we stained tissue for NeuN as a marker for cell bodies. Free-floating coronal sections were rinsed using 0.1 M PBS, incubated in blocking solution (containing 10% donkey serum and 0.3% Triton-X in 0.1 M PBS), and then incubated in primary antibody for 18–24 h (1 : 1000 anti-NeuN; Chemicon). The tissue was rinsed in 0.1 M PBS and subsequently incubated for 2–3 h in secondary antibody (1 : 500 donkey anti-mouse Alexa 647; Jackson Immunoresearch). The tissue was placed on slides, coverslipped (Vector Laboratories, Vectashield), and examined using a confocal microscope.

For sections within M1, we determined that about 71% of NeuN+ neurons near the injection site (range 52–85%; $n = 3$ animals) were also positive for ChR2, indicating that they expressed the virus. This included neurons in layers 2–6. This percent decreased with distance from the center of injection site. The promoter we used to drive viral expression, CaMKIIα, is largely specific for excitatory neurons (Dittgen et al. 2004; Nathanson et al. 2009). It is not known whether CaMKIIα is preferentially expressed in subpopulations of pyramidal neurons. However, ChR2 was present in the majority of neurons near the injection site, consistent with the assumption that the virus is being expressed nonselectively in M1 pyramidal neurons.

We examined S1 labeling in 8 slices from 3 animals for coexpression of NeuN and ChR2-mCherry. In a count of 4007 NeuN-positive cells distributed across cortical layers, we found 4 that also labeled with mCherry. Interestingly, the 4 retrogradely labeled neurons were found in layers 2/3. Owing to the sparse nature of the retrograde labeling (~1/1000 neurons), we concluded that any such labeling with this viral construct would be unlikely to affect our results. All of the data presented in this article were therefore collected from animals injected with the AAV2/5.CamKIIα.hChR2(H134R)-mCherry.WPRE.SV40 virus construct.

Preparation of in vitro S1 slices

Electrophysiological experiments began a minimum of 3 weeks following virus injection to allow for transport and full expression of the virus. At the time of experiments, the animals were 32–51 days of age. Mice were anesthetized with isoflurane, then the brain was removed and placed in ice-cold artificial cerebrospinal fluid (ACSF) containing (in mM): 126 NaCl, 3 KCl, 1.25 NaH_2PO_4, 2 $MgSO_4$, 26 $NaHCO_3$, 10 dextrose, and 2 $CaCl_2$, saturated with 95% O_2–5% CO_2. The tissue was then sliced at 400 μm in the coronal plane using a vibratome. Slices were incubated at 32 °C for 30–45 min and then maintained at room temperature until used for recording. Slices containing S1 barrel cortex were identified by the presence of layer IV barrels and a patchy barrel-related pattern of ChR2-mCherry fluorescence (Figs 1*B* and 2*A*). We recorded primarily from the larger, more medially situated barrels (rows D–E), as this is where fluorescence was typically strongest. We recorded from 1 to 3 adjacent barrels per slice.

Recording procedures

Whole-cell recordings were performed using glass micropipettes (4–10 MΩ) filled with internal solution containing (in mM): 135 κ-gluconate, 4 KCl, 2 NaCl, 10 HEPES, 0.2 EGTA, 4 ATP-Mg, 0.3 GTP-Tris, and 14 phosphocreatine-Tris (pH 7.25, 280–290 mOsm). Biocytin (0.5%) was added to the internal solution in a subset of experiments. Membrane potentials reported here were not corrected for the liquid junction potential. Recordings were conducted at 32 °C. When patching, cell-attached seal resistances were ≥1 GΩ and series resistance after achieving whole-cell configuration was 5–20 MΩ. After establishing whole-cell configuration, a series of current steps was presented in current clamp for use in characterization of cell type (see below). Current steps were presented in 20 pA steps, ranging from −100 to 300 pA. Steps were presented 5 s apart. In voltage-clamp experiments, series resistances ranged from 10 to 40 MΩ and were compensated for up to 80%. For excitatory postsynaptic current (EPSC) measurements, all cells were held at a potential of −80 mV. Data were collected using a Multiclamp 700B amplifier and pClamp10 software (Molecular Devices). Data were collected at a sampling rate of 20 kHz.

Cell-type identification

Cells were viewed under infrared-differential interference contrast illumination using a Nikon FN-1 microscope and a Dage IR-1000 CCD camera. In "GIN" mice, all of the GFP-expressing cells are inhibitory interneurons that express the neuropeptide somatostatin (SOM), although not all SOM+ interneurons are labeled with GFP (Oliva et al. 2000; Ma et al. 2006). Most or all of the GFP-expressing cells in this mouse line are morphologically consistent with Martinotti interneurons (Ma et al. 2006). GFP-expressing neurons are found in layers 2–5 but not in layer 6 (Ma et al. 2006), preventing us from positively identifying L6 SOM interneurons. All GFP-expressing interneurons were identified by visualization of GFP under epifluorescence illumination (Nikon Intensilight). All neurons identified in this study as "SOM" were labeled with GFP.

FS inhibitory interneurons do not express GFP in this mouse line. Therefore, cells with an oval-shaped soma were targeted as putative FS cells and their identity was confirmed based on electrophysiological characteristics (Beierlein et al. 2003; Fanselow et al. 2008). FS cells can exhibit different axonal projection patterns (Helmstaedter et al. 2009); therefore, our results may encompass FS cells with different morphologies. Nevertheless, a wealth of both in vitro and in vivo literature exists regarding the role of inhibitory interneurons identified as FS in cortical circuits. Our goal was to place our results regarding the role of FS inhibitory neurons in meditating M1-S1 interactions within the context of these findings.

Regular-spiking (RS) pyramidal cells were targeted for recording based on a triangular-shaped soma. During recording, RS pyramidal cells were similarly characterized based on established electrophysiological criteria (Porter et al. 2001; Beierlein et al. 2003; Hattox and Nelson 2007). We also recorded from a few pyramidal neurons in

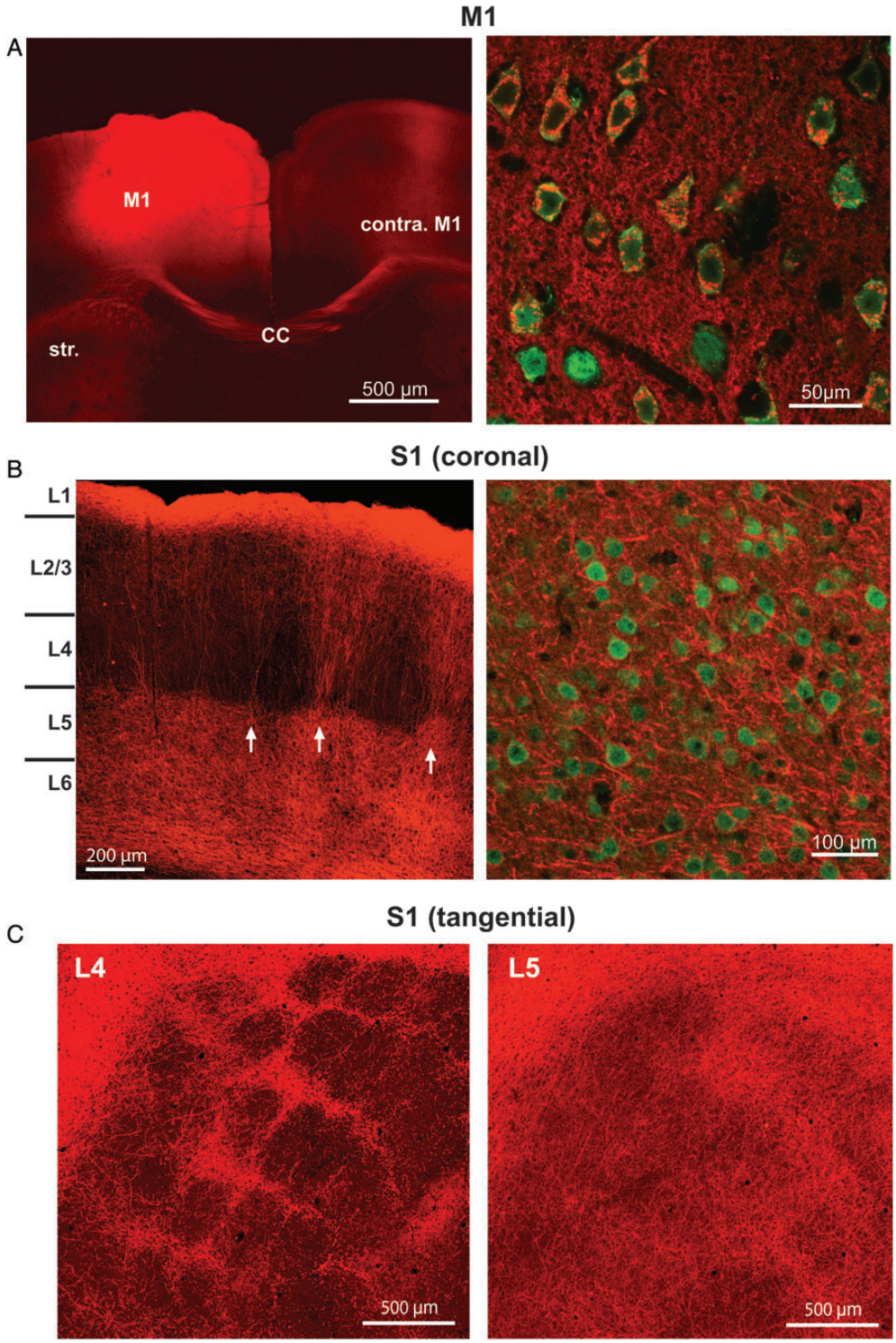

Figure 1. Injection of ChR2-mCherry viral vector produces extensive labeling of M1 axons within S1. (*A*) Left: Injection of the ChR2-mCherry viral vector produced robust fluorescent labeling around the injection site, shown here in the coronal plane. Projections from the injection site can be seen in contralateral M1 as well as the striatum. Str, striatum; CC, corpus callosum. Right: High-power magnification (×60) shows individual neurons, labeled with NeuN (green), co-expressing the ChR2-mCherry virus (red). (*B*) Left: ChR2-mCherry labeling of M1 axons within S1. Labeling pattern is typical of the termination pattern of M1 axons within S1. Arrows indicate septal columns of M1 fibers. Right: High-power magnification (×60) demonstrates that the ChR2-mCherry virus is only expressed in axons and axon terminals in S1, as no neurons in S1 (labeled with NeuN; green) are colabeled with ChR2-mCherry (red). (*C*) S1 sections cut in a plane tangential to the pial surface at depths corresponding to L4 (left) and L5 (right).

L5 that were not regular spiking, but instead displayed "intrinsically bursting" properties ($n = 3$). These cells showed similar results as the L5 RS cells, and were therefore pooled with the regular-spiking pyramidal (RS) neurons.

Laminar definitions

Layer 1 was identified by a low density of cell bodies, and the top of layer 2/3 was defined by the abrupt increase in cell density. The boundary between the bottom of L3 and the top of L4 was identified

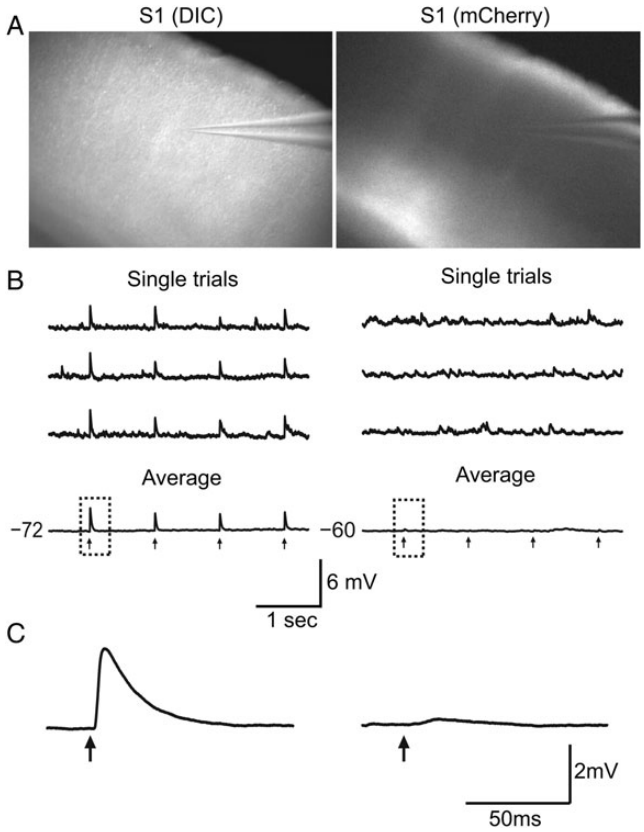

Figure 2. Optical stimulation of ChR2-expressing M1 axon terminals (ChR2-M1) results in time-locked excitatory responses in S1 neurons. (*A*) Left: In vitro brain slice through S1 under DIC at ×4 magnification. Right: Same brain slice under mCherry fluorescence shows robust ChR2-M1 labeling in S1. (*B*) Recording of single S1 pyramidal neurons during optical stimulation with 470 nm light (black arrows) evokes excitatory postsynaptic potentials (EPSPs) in some neurons (left) but not others (right). (*C*) Higher resolution traces of single optically evoked response shown in (*B*).

by the presence of barrels in L4, and the bottom of L4 was indicated by the loss of barrel structure as well as a more diffuse labeling pattern of fluorescent M1 axons. The boundary between layers 5 and 6 was approximated as being roughly half way between the top of L5 and the white matter. In a subset of our data, we measured the distance from the pia to the cell body of the recorded cell (see Fig. 6*A*). Based on these measurements, our laminar boundaries were very similar to previously published laminar definitions for S1 in the mouse (Hooks et al. 2011).

Optical stimulation procedures

To test for M1 input using optical stimulation, the recorded cell was centered in the field of view. Full-field blue light was delivered through a ×40 objective using a 470-nm LED (OptoLED; Cairn Research). Light intensity at the surface of the slice was ~20 mW/mm^2; light intensity was held constant across all experiments to minimize variability. This intensity is higher than the threshold for channelrhodopsin activation, which in our experiments as well as in previous studies is ~8–12 mW/mm^2 (Boyden et al. 2005). Keeping the light intensity stronger than the threshold for ChR2 activation allowed for reliable detection of synaptic connections within our experiments. Light intensity was measured using an optical power meter to measure the overall power and then dividing by the surface area of the light spot (to give mW/mm^2). We measured the spatial diameter of the light spot to be ~250 μm with some scattering of light beyond that. Consistent with this measurement, light-evoked responses were about 50% of the maximal response when stimulated 250 μm from the neuron's somata. This indicates the activation range probably extends ~1 barrel-related column in width, or perhaps slightly more. Light stimulation was delivered via TTL pulses using the pCLAMP software. A single stimulation trial consisted of trains of 8–10 pulses (each pulse was 1.0 ms duration) at 1, 10, 20, and 40 Hz, with trains separated by >8 s to minimize adaptation effects. For each cell, 10–30 trials were recorded.

We took multiple steps to limit experimental variability arising from variation in the amount of virus taken up and/or expressed across animals. First, we only recorded from slices exhibiting strong ChR2-mCherry expression that was easily visible under ×4 magnification (e.g., Fig. 2*A*). Second, we limited recordings to the area in barrel cortex having the highest ChR2-mCherry expression; this was typically 1–3 medially situated adjacent barrels. Third, we included data only from animals in which at least one significant excitatory response was identified. Fourth, we attempted to sample multiple cells within each slice such that the sample contained a variety of cell types from different layers.

Data analysis

Data were analyzed using in-house programs written in Matlab (The MathWorks, Natick, MA, USA; A. Kinnischtzke). Trials were averaged together, and analyses were performed on averaged voltage traces. Response onset and peak were calculated within a 15-ms window following the offset of the light pulse. Response onset was taken as the first of 20 consecutive data points that exceeded a threshold of 1 SD above the resting membrane potential. A cell was considered to have received an input if the peak response was >5 times the standard deviation of the resting membrane potential. Excitatory postsynaptic potential (EPSP) and EPSC amplitudes were calculated as the difference between the response onset and the peak response. In cases where a cell spiked in current-clamp mode, the peak response was taken to be the action potential voltage threshold. For analysis of synaptic dynamics, response amplitudes were calculated using EPSCs, and we used only cells that had a significant response to the first pulse in the train. Response amplitudes were calculated for each pulse then normalized to the first value.

For comparison of input probabilities between cell types or layers, we used a χ^2 test. For all other statistical comparisons, an ANOVA was performed for each data set and *t*-tests were used for post hoc pairwise comparisons. Results are reported as mean ± SEM.

Results

Anatomy of the M1–S1 projection

To study synaptic inputs from M1 to identified S1 neurons, we injected an AAV virus containing the channelrhodopsin-2 (ChR2) gene into primary motor cortex (see Materials and Methods section; Fig. 1*A*, left). Experiments were performed a minimum of 3 weeks following the injection, at which time pyramidal neurons in M1 showed strong expression of ChR2 (Fig. 1*A*, right). Viral expression was primarily located in M1 neurons within the agranular medial field (vibrissal motor cortex) with some in the agranular lateral cortex (Brecht et al. 2006). This produced a stereotypical pattern of axonal labeling within S1 (Fig. 1*B*) that was consistent with known patterning of M1 axons (Veinante and Deschenes 2003; Petreanu et al. 2009). This pattern of labeling was consistent across animals; however, we observed some variability between animals in the amount of ChR2 labeling that was present (see Materials and Methods section). Layers 5 and 6 (L5 and L6) were characterized by diffuse labeling. At the L4/L5 boundary, labeling became concentrated within vertical bands that coursed through L4 and L2/L3. Labeling broadened somewhat before becoming extensive and widespread in L1 (Fig. 1*B*). The vertical bands of M1 fibers appeared to be concentrated

between barrel centers, which were largely devoid of M1 axons. To explore this further, we sliced through the S1 barrel field in the tangential plane to highlight barrel versus septal areas. We found that in L4, M1 labeling was concentrated primarily between the barrels, within the septa (Fig. 1*C*, left). In deeper layers, as was observed in the coronal slice, M1 axons became more diffuse; however, they remained more concentrated under the septa all the way through L5 and L6 (Fig. 1*C*, right).

M1 provides input to excitatory and inhibitory neurons in S1

In order to test for M1 input to individual neurons in S1, we optically stimulated the ChR2-expressing M1 axon terminals while recording from a neuron in S1 (Fig. 2*A*). We determined whether the recorded cell received M1 input by stimulating with trains of light pulses (Fig. 2*B*). Cells deemed to have an evoked response showed time-locked EPSPs that were typically present following every individual pulse; that is, they displayed little synaptic failure. Excitatory responses were readily observed when averaged across trials (Fig. 2*B* and *C*, left). Occasionally, an inhibitory response was observed as well (see below). In a subset of cells, we computed the latency to EPSP onset on each trial (10–30 trials per cell) and averaged the values for each cell (3.21 ± 0.41 ms; $n = 5$ cells). To determine the trial-to-trial "jitter" in the EPSP response onset, for each cell, we calculated the coefficient of variation (CV) of the EPSP onset latency across trials. The mean CV was 0.09 ± 0.02 ($n = 5$ cells). Because variability between trials was low, we calculated an average EPSP for each cell and performed subsequent analyses on such trial-averaged responses. The trial-averaged EPSP latency for all cells ($n = 95$) was 2.99 ± 0.09 ms.

In order to verify that the short-latency responses were monosynaptic, we performed a series of experiments where we included 1 μM tetrodotoxin (TTX) and 1 mM 4-aminopyridine (4-AP) in the bath to block sodium and potassium channels, respectively (Petreanu et al. 2009; Cruikshank et al. 2010). In the presence of TTX only, M1-evoked responses were always abolished (data not shown; $n = 11/11$ cells). When we additionally added 4-AP, to enhance indirectly the depolarizing effects of ChR2, evoked responses were present in most cells (data not shown; $n = 11/13$). When responses remained in the presence of TTX and 4-AP, for all cells ($n = 11/11$), the M1-evoked response latency was significantly longer than under control conditions (control: 3.13 ± 0.04 ms; TTX + 4-AP: 6.46 ± 0.09 ms; $P < 0.005$). Also, almost all neurons ($n = 10/11$) exhibited reduced M1-evoked response amplitudes in the presence of TTX and 4-AP, although this decrease was not significant (control: 6.87 ± 0.33 mV; TTX + 4-AP: 3.80 ± 0.33 mV; $P = 0.08$). The cells tested with TTX and 4-AP included all 3 cell types examined in this study (see below) and the effects of TTX and 4-AP did not depend on cell type. These results are consistent with previous findings (Cruikshank et al. 2010) and illustrate that the light-evoked excitatory responses we observed are directly postsynaptic to ChR2-expressing M1 axon terminals.

Previous work demonstrated that M1 inputs directly contact pyramidal neurons within L2/L3 and L5 of somatosensory cortex (Petreanu et al. 2009; Mao et al. 2011; Rocco-Donovan et al. 2011). We wanted to determine here whether M1 also provides synaptic input onto inhibitory interneurons. We therefore recorded from 3 cell types within S1: RS neurons, FS inhibitory interneurons, and SOM inhibitory interneurons (Fig. 3*A*). RS and FS neurons were identified using established electrophysiological criteria (see Materials and Methods section), and SOM interneurons expressed GFP. In addition, we recorded from a population of neurons that could not be readily categorized into 1 of these 3 groups yet were too heterogeneous to comprise a meaningful fourth cell type ("nonclassified" cells).

We found that in addition to contacting pyramidal neurons with a high probability ($n = 56/74$), M1 also provided input to FS interneurons ($n = 10/17$) and SOM inhibitory interneurons ($n = 18/27$). Connection probabilities were equivalent among the cell types ($P = 0.32$; Fig. 3*C*). The latency of the evoked responses also did not differ between the 3 cell types (RS: 2.97 ± 0.02 ms; FS: 2.61 ± 0.07 ms; GIN: 3.08 ± 0.04 ms; $P = 0.42$). The "nonclassified" cells also received input from M1 ($n = 9/16$; data not shown). The characteristics of the M1

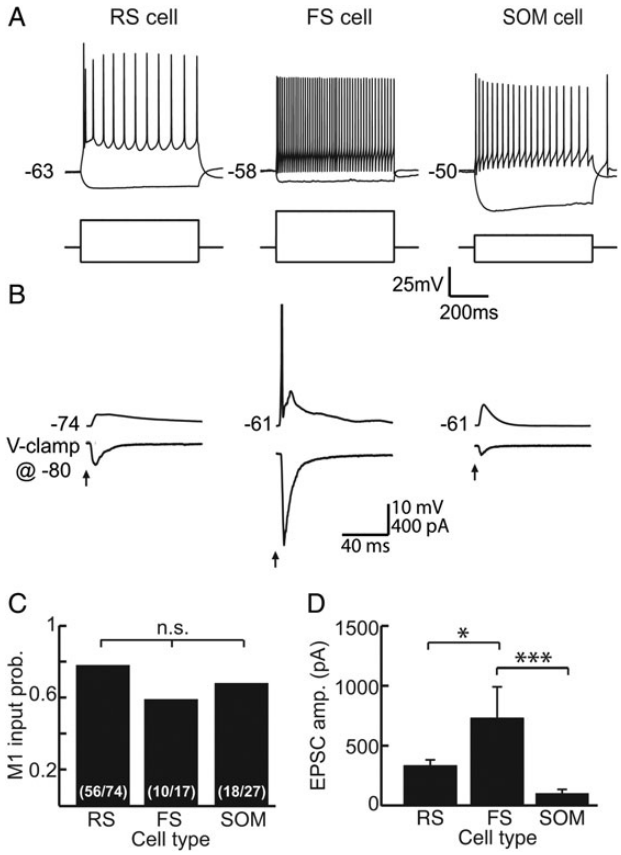

Figure 3. M1 contacts 3 major cell types in S1. (*A*) Example traces identifying a regular-spiking (RS) pyramidal neuron (left), a fast-spiking (FS) inhibitory interneuron (middle), and a somatostatin-expressing (SOM) inhibitory interneuron (right). Each cell type exhibits characteristic voltage responses (top) to hyperpolarizing and depolarizing current step injections (bottom). (*B*) Example traces for an RS cell (left), FS cell (middle), and SOM cell (right) demonstrating excitatory responses to optical stimulation of ChR2-M1 fibers. Responses were measured in current clamp (top) and voltage clamp (bottom). Holding potential for voltage clamp was −80 mV for all recordings. Note that the FS cell spiked. (*C*) Quantification of the probability of receiving an input from M1 by cell type demonstrates equivalence among them ($P = 0.32$). (*D*) Amplitudes of excitatory currents evoked by ChR2-M1 stimulation are significantly greater in FS than RS ($P < 0.05$) and SOM cells ($P < 0.005$). Amplitudes do not differ between RS and SOM cells ($P > 0.05$). Panels *C* and *D* contain cells recorded from layers 2 though 6.

inputs to the nonclassified neurons were not distinct and fell within the range observed for our 3 identified cell types; therefore, we opted to not include these cells in further analyses. Overall, these results suggest that M1 afferents do not discriminate by cell type, but instead provide direct input to most types of cells within S1.

We compared the strength of excitatory responses among cell types. We found that although all 3 cell types had a similar probability of receiving M1 input, the strength of the inputs differed among them (ANOVA $P = 0.0012$; Fig. 3*D*). The average amplitude of EPSCs onto FS cells was the largest (730.29 ± 261.1 pA), and this was significantly greater than that of the M1 input onto RS cells (321.83 ± 52.8 pA; $P < 0.05$) or SOM cells (84.43 ± 28.8 pA; $P < 0.005$). This demonstrates that M1 strongly contacts FS cells, which could evoke robust disynaptic inhibition within S1 (see below).

Short-term dynamics of M1 inputs are dependent on postsynaptic cell type

Both thalamocortical (TC) and local cortical inputs onto RS, FS, and SOM cells exhibit distinct short-term dynamics that are dependent on the identity of the postsynaptic cell. To determine if M1 inputs show short-term synaptic depression or facilitation, we stimulated the ChR2-expressing M1 terminals with trains of light pulses at 1 and 10 Hz (Fig. 4). The dynamics of the M1 input depended on the postsynaptic cell type. With 10-Hz trains, the magnitude of the EPSCs displayed short-term depression in the RS cell and FS cell populations and short-term facilitation in the SOM population (Fig. 4*A* and *B*). The time course of short-term depression in the RS and FS cell populations was similar at 1 and 10 Hz (Fig. 4*B*).

We also recorded in current clamp and examined the change in the probability of eliciting spikes across the stimulus train (Fig. 4*A*,*C*,*D*). Out of the cells in each cell type that spiked at least once (16/56 RS cells; 6/10 FS cells; 10/18 SOM cells), the probability of eliciting a spike across the train tended to increase in SOM cells and decrease in the RS cells, although the change was variable in both populations (data not shown). The incidence of spiking is consistent with SOM cells displaying short-term facilitation and RS cells exhibiting short-term depression (Fig. 4*B*). In FS cells, although EPSC responses displayed synaptic depression, we observed spiking in response to each pulse across the 10 Hz train. This is likely due to the large amplitude EPSCs evoked in FS cells (Fig. 3*D*) under these conditions.

When we compared all cells receiving M1 input for each cell type under equivalent recording conditions (i.e., same light intensity for stimulation), FS cells ($n = 10$) were significantly more likely to spike to both the first pulse (0.64 ± 0.16; Fig. 4*C*) and fifth pulse (0.63 ± 0.16; Fig. 4*D*) in a 10-Hz train than RS (first pulse: 0.12 ± 0.04, fifth pulse: 0.09 ± 0.03; $P < 0.005$) or SOM (first pulse: 0.10 ± 0.06, $P < 0.01$; fifth pulse: 0.19 ± 0.07, $P < 0.005$) cells. This is consistent with our previous finding that FS cells receive stronger excitatory drive from M1 than RS or SOM cells and likely produce feedforward inhibition onto S1 neurons.

Feedforward inhibition recruited by M1 stimulation

We observed a high probability of spiking in the FS cell population, indicating that M1 activation could recruit widespread disynaptic inhibition within S1. To test this possibility, we recorded in voltage clamp and held the cells at a potential of −20 mV to determine the presence or absence of an inhibitory postsynaptic current (IPSC; Fig. 5). We observed IPSCs in RS cells, FS cells, and SOM cells that appeared delayed relative to the initial EPSC (Fig. 5*A*). We found that, for each cell type, a high proportion of the cells that received excitatory input from M1 also displayed a disynaptic inhibitory response (66% of RS cells, 60% of FS cells, 65% of SOM cells; Fig. 5*B*). The peak of the IPSC followed the peak of the EPSC in nearly all cells ($n = 36/38$; average delay was 4.89 ± 0.57 ms). The IPSC–EPSC peak delay was slightly less in FS cells (3.76 ± 1.07 ms) than RS (4.99 ± 0.77 ms) or SOM cells (4.97 ± 1.02 ms); however, there was no significant difference among cell types ($P = 0.85$). In contrast to the short-term dynamics of the M1 excitatory inputs, the disynaptic inhibitory responses showed short-term depression in all 3 cell types (Fig. 5*C*). This suggests that M1 activation generates extensive inhibition

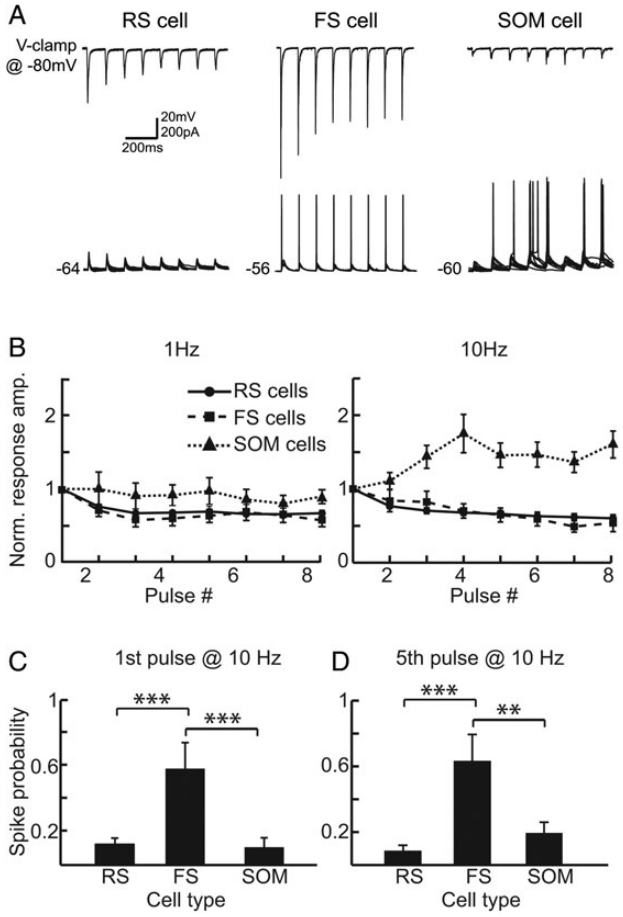

Figure 4. Responses to ChR2-M1 optical stimulation exhibit cell-type-dependent short-term synaptic dynamics. (*A*) Example traces in voltage clamp (top) and current clamp (bottom) demonstrate changes in excitatory response amplitudes and spike probability for RS cells (left), FS cells (middle), and SOM cells (right) across a train of optical stimuli at 10 Hz. Voltage-clamp traces show averaged responses whereas current-clamp traces show multiple single trials overlaid. (*B*) EPSC responses are normalized to the response amplitude evoked by the first pulse for RS cells (solid line; circles), FS cells (dashed line; squares), and SOM cells (dotted line; triangles) at both 1 Hz (left) and 10 Hz (right). (*C*) For the first pulse in a 10 Hz train, stimulation of ChR2-expressing M1 terminals resulted in significantly greater probability of spiking in FS than RS cells ($P < 0.005$) and SOM cells ($P < 0.005$). (*D*) Spiking probability was also greater in FS than RS cells ($P < 0.005$) and SOM cells ($P < 0.01$) for the fifth pulse in a 10-Hz stimulation train. Data in (*C*) and (*D*) consist of all cells receiving M1 input.

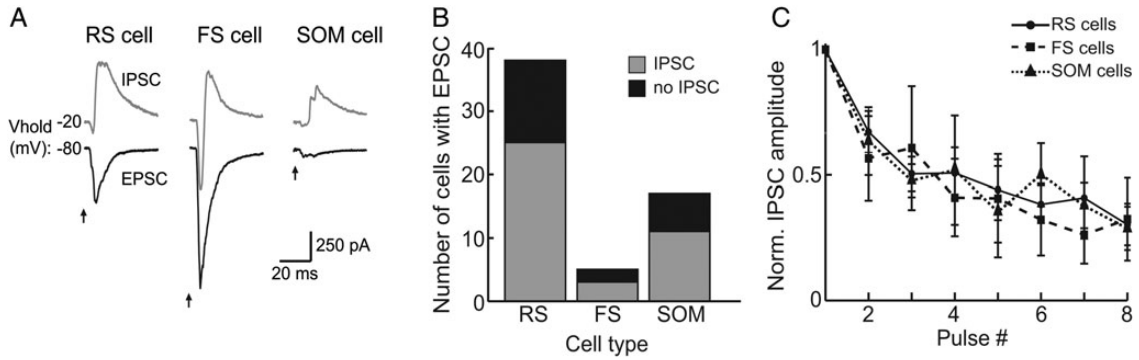

Figure 5. Optical stimulation of ChR2-M1 terminals evokes widespread disynaptic inhibition in RS cells, FS cells, and SOM cells within S1. (*A*) Examples of excitatory and inhibitory postsynaptic currents (EPSCs and IPSCs) in RS cells (left), FS cells (middle), and SOM cells (right) in response to ChR2-M1 stimulation. Cells were held at −80 mV for EPSC recordings and −20 mV for IPSC recordings. (*B*) Summary of number of neurons with both EPSC and IPSC responses by cell type. (*C*) Normalized IPSC amplitudes for RS cells (sold line; circles), FS cells (dashed line; squares), and SOM cells (dotted line; triangle) for a 10-Hz optical pulse train.

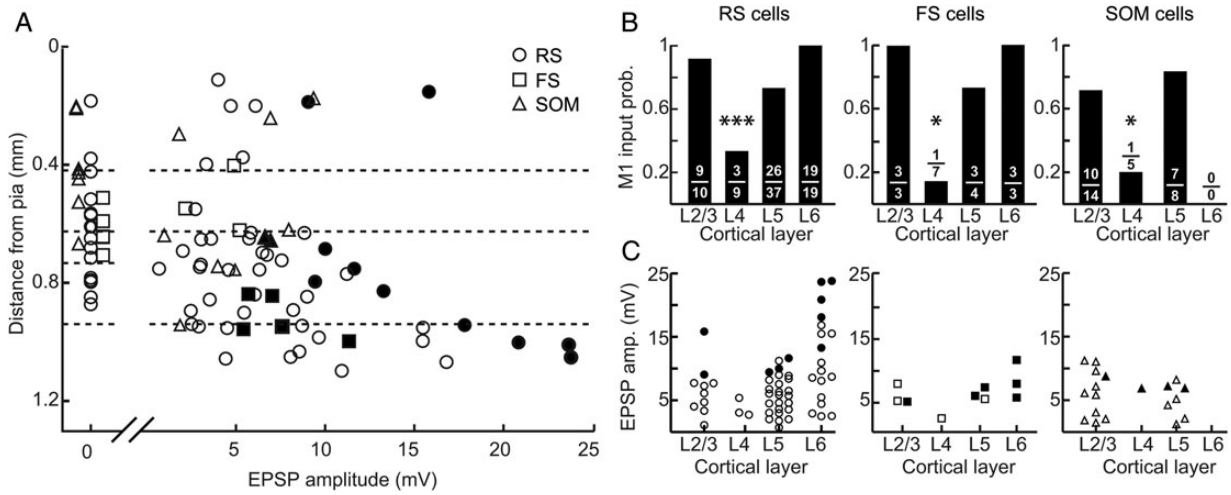

Figure 6. M1 inputs to excitatory and inhibitory neurons in S1 exhibit similar laminar distributions. (*A*) Amplitude of M1 input as a function of depth from pia. Each point represents EPSP amplitude in response to ChR2-M1 stimulation for individual cells (circles: RS cells; squares: FS cells; triangles: SOM cells). Dashed lines indicate laminar boundaries and were placed as follows (in μm from pia): L2/L3–L4: 419; L4–L5: 626; L5–L6: 940. Data plotted are a subset of data shown in (*B*) and (*C*). Filled circles represent cells that spiked in response to ChR2-M1 on at least 2 trials; open circles are cells that did not spike. (*B*) Probability of receiving an M1 input by layer for RS cells (left), FS cells (middle), and SOM cells (right). Numbers represent the number of cells that received input out of total number of cells recorded for that layer and cell type. (*C*) EPSP amplitude of evoked response to ChR2-M1 optical stimulation as a function of layer for RS cells (left; circles), FS cells (middle; squares), and SOM cells (right; triangles). Conventions as in (*A*).

within S1 that depresses at frequencies of ≥10 Hz. That FS cells are the most likely to be driven suprathreshold by M1 stimulation strongly suggests that this inhibition is mediated by FS interneurons.

Laminar dependence of M1 input

The pattern of ChR2-M1 axons was distinctly nonuniform across S1 cortical layers (see above; Fig. 1). We therefore examined in a subset of cells whether particular layers within S1 receive more M1 input than others and whether this depends on cell type (Fig. 6*A*). The probability of a cell receiving an M1 input was lowest in L4 (~20%), and this was the case for all 3 cell types (RS: $P = 0.0008$, FS: $P = 0.016$, SOM: $P = 0.037$; Fig. 6*B*). In each of the other layers, input probability was ~80% for each cell type. We similarly examined response amplitudes (EPSPs). For all S1 neurons we recorded, there was a significant difference in response magnitude across layers (ANOVA $P < 0.005$; data not shown). When we separated the data by cell type, RS amplitudes differed significantly by laminar location (ANOVA $P = 0.0011$). Laminar dependency was at best at trend level for FS (ANOVA $P = 0.18$), and SOM cells did not display laminar differences (ANOVA $P = 0.82$). In both RS and FS cells, excitatory responses were largest in L6 as was the proportion of cells that fired action potentials. In RS cells, L6 response amplitudes were on average significantly larger than in the other layers ($P < 0.05$). We were unable to determine whether SOM interneurons also receive their strongest M1 inputs in L6 because there are no GFP+ cells in L6 of GIN mice; SOM cells do exist there, however (Markram et al. 2004; Ma et al. 2006; Lee et al. 2010).

We found unexpectedly that M1 inputs were especially large in a subset of L6 cells. To verify that these results were not an artifact of between-animal variability in ChR2 expression or activation (see Materials and Methods section), we recorded sequentially from RS neurons in L5 and L6 within the same slice (Fig. 7). Pairwise comparison of L5 and L6 RS cells showed that L6 cells indeed receive, on average,

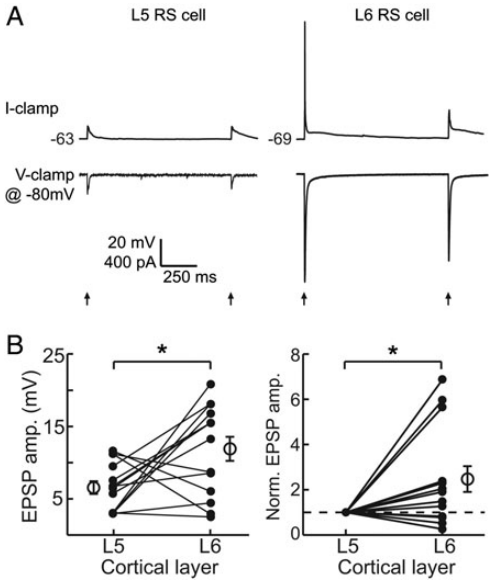

Figure 7. Optical stimulation of ChR2-expressing M1 terminals within S1 evokes stronger responses in L6 cells than in L5 cells. (*A*) Example traces in current clamp (top) and voltage clamp (bottom) of a L5 RS neuron (left) and a L6 RS neuron (right) recorded from the same slice. (*B*) Average M1 response amplitudes for paired L5 and L6 RS cells within the same slice (left; $P < 0.05$, paired *t*-test). Same data normalized to the amplitude of the L5 cell (right; $P < 0.05$, *t*-test). Filled circles represent individual cells and open circles and bars represent the mean and SEM for each population.

significantly larger M1 inputs ($P = 0.02$; Fig. 7*B*, left) although the difference was not necessarily observed in every pair. When we normalized the paired data to the amplitude of the L5 cell, it was clear that relative to nearby L5 neurons a subset of neurons in L6 receive especially strong M1 input (mean normalized L6: 2.47 ± 0.57, $P = 0.02$; Fig. 7*B*, right). Interestingly, it appears that the L6 cells having the largest responses are concentrated in upper L6, near the L5/L6 border (Fig. 6*A*). The cells receiving large M1 inputs exhibited regular-spiking characteristics, as did all L6 pyramidal neurons; however, they did tend to show an initial spike "doublet" in response to current step injection, whereas L6 pyramidal neurons receiving less M1 input did not. These results suggest they could represent a specific class of projection neurons (Otsuka and Kawaguchi 2011) that remain to be identified in future studies.

Discussion

Here, we took advantage of optogenetic tools to investigate motor cortex to somatosensory cortex synaptic circuitry. By injecting an AAV vector carrying the ChR2 gene into M1, we were able specifically to investigate properties of anterograde connections from M1 to S1. Provided that ChR2 is transported only anterogradely, our experimental approach avoided confounds associated with inadvertent synaptic activation by local recurrent axons in S1. We verified that labeling was indeed virtually entirely anterograde in nature (see Materials and Methods section).

Our experiments yield four important findings. First, M1 inputs engage 3 main types of S1 neurons, including 2 classes of inhibitory interneurons as well as excitatory pyramidal neurons. As a consequence, M1 activation produces both direct excitation as well as substantial disynaptic inhibition within S1. Second, motor cortex inputs to pyramidal neurons, FS and SOM inhibitory interneurons possess cell-type-specific synaptic dynamics. The dynamics are similar to those of other extrinsic and intrinsic inputs, including TC and local corticocortical connections. Third, M1 input to excitatory and inhibitory neurons display similar laminar distributions. Regardless of cell type, neurons in L4 were the least likely to receive input from motor cortex, whereas all 3 cell types in other layers showed a similar, high probability of M1 input. Fourth, M1 labeling is distributed into vertically oriented columns that are complementary to those described for TC inputs from the ventral posteromedial (VPm) thalamic nucleus, the major subcortical station in the whisker-to-barrel pathway. Taken together, our findings suggest that M1 exerts on S1 modulatory excitatory and inhibitory effects that may differentially influence corticocortical versus TC processing streams.

Selective stimulation of M1 axons with channelrhodopsin

Use of optogenetic techniques allowed for sole activation within S1 of axons originating from primary motor cortex. Such specificity has been difficult to achieve with traditional electrical stimulation techniques, as unintentional antidromic activation of fibers in reciprocally connected brain regions, such as S1 and M1, is difficult to avoid. In addition, we were able to activate ChR2-expressing fibers directly within S1 as opposed to the neuronal somata in M1. This allows greater confidence for detecting the presence of synaptic connections, as the entire axon tract need not be preserved within the slice. Under these conditions, the latency measure likely reflects primarily the synaptic delay of neurotransmitter release from the presynaptic ChR2-expressing terminal to the postsynaptic neuron.

Wide-field optical stimulation, as we used in this study, likely produces synchronous or near-synchronous activation of all or most of the ChR2-expressing M1 terminals within the activated region, a condition that could correspond to the upper bound of S1 engagement by M1. While our stimulation protocol may not be analogous to physiological M1 activity, it enabled us to identify connections that may not have been apparent with weaker stimuli. Importantly, our approach provided the opportunity to identify similarities, such as feedforward inhibition, and differences, that is, direct engagement of SOM cells, in afferent cortical circuitry, notably that associated with thalamic input (see below).

Further investigation into the strength of unitary connections, as opposed to population connections, will provide additional insight into whether the large inputs to some S1 neurons result from stronger synaptic connections and/or a convergence of more synapses onto single postsynaptic neurons. Traditional in vitro experimental paradigms, such as minimal stimulation techniques, could be adapted for use with optical stimulation to address these questions in future studies. Nevertheless, our findings are consistent with other results demonstrating that FS cells receive large TC and corticocortical inputs. Previous studies have demonstrated for these inputs that FS cells receive larger unitary inputs than RS cells (Cruikshank et al. 2007) or SOM cells (Beierlein et al. 2003); it seems likely that the same could be true for M1 inputs onto FS interneurons.

Motor cortex input to inhibitory and excitatory neurons in S1

At a population level, motor cortex neurons contact 3 major types of S1 neurons with high probability. Indeed, up to 80% of recorded S1 cells displayed short-latency excitatory responses. The strongest M1 inputs are to FS inhibitory neurons. This was evident in both the size of the excitatory currents and the likelihood that these inputs evoked FS spikes. Our finding that FS interneurons overall receive the strongest M1 input could be a reflection of the greater recruitment of FS interneurons located in deeper layers (see below). That FS cells receive large excitatory input is reminiscent of the synaptic properties of TC inputs to FS cells in layer 4 barrels (Porter et al. 2001; Beierlein et al. 2003; Cruikshank et al. 2007). SOM inhibitory interneurons also have a high probability of receiving M1 input, but the amplitude of the responses and the probability of spiking were substantially smaller. SOM inhibitory interneurons have high input resistances and depolarized resting potentials (Fanselow et al. 2008; Kinnischtzke et al. 2012). However, despite their greater intrinsic excitability relative to FS interneurons, the probability of eliciting action potentials with M1-ChR2 activation was much lower at the stimulation frequency used here. Together, these M1–S1 findings parallel those showing strong input from local S1 excitatory neurons onto FS interneurons and weak input onto SOM interneurons (Markram et al. 1998; Xiang et al. 2002; Beierlein et al. 2003; Thomson and Lamy 2007). Thus, the distinctive synaptic profiles of FS and SOM interneurons extend to at least one long-range, interareal corticocortical system.

Given the high convergence of FS cells onto local excitatory neurons in S1 (Thomson and Lamy 2007; Oswald et al. 2009; Packer and Yuste 2011), strong activation of FS cells by motor cortex is likely to result in widespread disynaptic inhibition within S1. We determined the presence or absence of disynaptic IPSCs following M1 stimulation, and indeed found that when an S1 neuron of any cell type received an excitatory M1 input, it was usually followed by an IPSC. Based on our findings with FS and SOM inhibitory cells, we hypothesize that this disynaptic inhibition originates from FS cells. We also recorded from nonclassified neurons. This group likely contains inhibitory neurons that were neither GFP+ (identifying them as SOM-expressing) nor conclusively FS interneurons, such as VIP-expressing, CCK-expressing, or neurogliaform cells (Markram et al. 2004; Lee et al. 2010). Because the nonclassified cells also received input from M1 (data not shown), it is possible that these additional inhibitory interneuron classes may also be involved in mediating the IPSCs observed here. This could also vary by depth, as the relative abundance of these inhibitory interneuron groups varies across S1 layers (Lee et al. 2010). However, given the high spiking probability that we observed in FS cells, M1-evoked inhibition in our preparation most likely originated from the FS inhibitory neurons. Direct, efficacious TC inputs to FS cells also provide strong, fast disynaptic inhibition for processing sensory signals (Cruikshank et al. 2007). Thus, FS interneurons generate fast, reliable inhibition in response to thalamic, local corticocortical, and M1 signals.

Pyramidal neurons in S1 show considerable diversity in terms of their morphology, intrinsic biophysical properties, projection targets, sources of excitatory input, and response properties (e.g., Swadlow 1989; Elhanany and White 1990; Agmon and Connors 1992; Hattox and Nelson 2007). Given this diversity, we were somewhat surprised by the lack of discernible groups of pyramidal neurons in terms of their M1 inputs. With the exception of some L6 cells (see below), responses tended to be subthreshold (usually <10 mV). These inputs appear to be smaller than those of the reciprocal S1 to M1 projection (Mao et al. 2011; Rocco-Donovan et al. 2011). These findings suggest that M1 provides weak excitation to L2/3 and L5 pyramidal neurons in S1 regardless of their projection target, as well as to many L6 pyramidal neurons. This conclusion is consistent with recent findings that L2/3 and L5A M1-projecting pyramidal neurons in S1 receive similar magnitudes of M1 input as nearby pyramidal neurons projecting to other targets (Mao et al. 2011). M1 may therefore provide a general increase in excitation to the majority of pyramidal neurons in S1, with a subset of L6 pyramidal cells being the exception.

Synaptic dynamics of M1 inputs onto neurons in S1

A striking feature of SOM interneurons is how the efficacy of their excitatory synaptic inputs changes with repeated stimulation. Local corticocortical synapses to SOM cells facilitate, whereas excitatory inputs to RS and FS cells depress. We observed qualitatively similar effects here. In response to periodic M1-ChR2 stimulation, RS and FS cells exhibited short-term depression similar to that observed for TC (Beierlein and Connors 2002; Chung et al. 2002; Cruikshank et al. 2007) and local intracortical synapses (Markram et al. 1998; Reyes et al. 1998; Oswald and Reyes 2008, 2011). These findings indicate that the distinct synaptic dynamics that apply to FS versus SOM inhibitory interneurons extend to long-range cortical inputs, such as from primary motor cortex. Because SOM cells exhibit short-term facilitation, it has been suggested they provide a delayed source of inhibition in the presence of sustained high-frequency inputs (Pouille and Scanziani 2004; Kapfer et al. 2007; Silberberg and Markram 2007). We did not measure responses at frequencies above 10 Hz, as we observed at frequencies ≥20 Hz a larger probability of response failure as well as a summation of postsynaptic responses. This could be a result of using ChR2 as opposed to electrical stimulation, as ChR2 has relatively slow recovery from inactivation and can continue to conduct for a few milliseconds following removal of the light stimulus (Nagel et al. 2003; Cruikshank et al. 2010; Gunaydin et al. 2010). M1 inputs to SOM cells may continue to facilitate at higher frequencies, as occurs at local RS to SOM synapses (Fanselow et al. 2008), which could lead to greater recruitment of SOM interneurons.

Synaptic depression in RS and FS cells at 10 Hz was modest, particularly considering that channelrhodopsin tends to slightly exaggerate the degree of synaptic depression compared to electrical stimulation (Cruikshank et al. 2010). Nevertheless, our data are consistent with the idea that M1–S1 synapses depress less than TC synapses. Using a similar optogenetics approach, Cruikshank et al. reported greater synaptic depression at TC-FS and TC-RS synapses than we find at M1-FS and M1-RS synapses. M1 inputs may therefore be more similar to local corticocortical synapses, which are generally thought to exhibit less synaptic depression than TC synapses (Gil et al. 1997; Beierlein et al. 2003). Together, findings raise the interesting possibility that the intrinsic nature of synaptic

depression reflects the spiking statistics of the presynaptic neurons. That is, populations associated with high firing rates may have more depressing synapses than those associated with lower firing rates. In this regard, in vivo firing of VPm neurons is likely higher than that of cells in S1. Correspondingly, for equivalent stimulation frequencies, TC synapses display more depression than S1 synapses. In addition, overall in vivo firing frequencies of M1 neurons projecting to S1 may be lower than those of VPm cells, and this may be reflected in the tendency for M1-S1 synapses to exhibit less short-term synaptic depression.

Laminar and columnar organization of M1 input to S1

Our anatomical data demonstrate that L4 is largely devoid of M1 axons, particularly within barrel centers. In accordance with this, neurons in L4 were the least likely to receive input from M1 (Fig. 6). This was true for all 3 cell types: RS excitatory cells, FS inhibitory neurons, and SOM inhibitory interneurons. L4 is the primary input layer for TC axon terminals to S1 from VPm (Killackey 1973). Because we observed relatively few M1 contacts to L4 neurons, we conclude that M1 is unlikely to directly modulate VPm inputs within L4. Furthermore, S1 neurons that project back to M1 are similarly scarce in L4 (Alloway et al. 2004). Therefore, during active whisking M1 may modulate S1 in a layer-specific manner (Krupa et al. 2004), with signal processing in L4 occurring largely independently of direct M1 influences.

Motor cortex axons terminate in a distinct pattern within S1, wherein the axon from a single M1 neuron terminates extensively within L5 and L6 before traveling vertically and ramifying within L1 (Veinante and Deschenes 2003). We observed the same pattern of ChR2 labeling (Figs 1 and 2). M1 projections were vertically concentrated in columns interposed between barrel-related columns, particularly in L4. In rats, M1-projecting pyramidal neurons are also concentrated in vertical columns within interbarrel septa (Alloway et al. 2004). VPm-related circuits in L4 and L6 are more barrel-focused than inputs from the thalamic posteromedial (POm) nucleus, which target interbarrel septa (Chmielowska et al. 1989; Wimmer et al. 2010). Present findings thus provide further evidence for a vertical organization within the whisker area of S1 in which barrel- and septal-related columns represent different information streams and/or different modes of sensorimotor integration. As suggested by others (Alloway 2008), septal-related columns may be more tightly coupled to the motor system.

Pyramidal cells in L6 exhibited more heterogeneity in their M1 input amplitudes than pyramidal neurons in any of the other layers (Fig. 6). On average, L6 pyramidal neurons had significantly larger M1 inputs. This was due to a subset of cells that received exceptionally strong inputs; unlike other pyramidal cells, these often spiked. Pyramidal neurons in L6 are heterogeneous in their projections (Zhang and Deschenes 1997). Perhaps M1 strongly contacts a particular class of L6 neurons, such as those projecting to a specific target (e.g., VPM, POm, M1, etc.).

M1 input magnitudes to pyramidal neurons are progressively larger in deeper layers, particularly at the border of L5 and L6 (Fig. 6*A*). Interestingly, the inputs to FS cells scaled similarly. FS cells in L5 and L6 received strong M1 inputs, and most of them reliably fired action potentials in response to ChR2 stimulation. Although SOM cells constitute a major portion of inhibitory interneurons within L6 (Markram et al. 2004; Lee et al. 2010), in our mouse line SOM cells in L6 are not labeled with GFP (Ma et al. 2006), and we were therefore unable to identify and record from SOM-expressing interneurons in L6. However, our findings with the FS cells provide evidence that M1 recruits strong inhibition within the deeper layers that parallels strong, direct excitatory input from M1.

Functional Significance

Our findings demonstrate that M1 broadly engages S1 circuits and, further, that M1 inputs onto pyramidal neurons are widespread but usually subthreshold. TC recipient zones seem to be the exception, with L4 barrel centers receiving few inputs and upper layer 6 receiving especially strong ones. Our findings thus suggest that M1 targets multiple pyramidal cell populations that participate in a variety of local circuits and that collectively project to a broad range of cortical and subcortical targets. M1 neurons also directly contact at least 2 major types of inhibitory neurons and possibly other types.

M1 neurons abruptly increase their firing prior to the onset of whisking and many continue to fire tonically throughout the whisking bout (Carvell et al. 1996; Friedman et al. 2006, 2012). Present results show that M1 activates fast feedforward inhibition, likely via FS inhibitory interneurons, in a manner similar to that of TC inputs to layer 4 of barrel cortex. There, feedforward inhibition creates a "window of opportunity" for L4 neurons to spike, producing a robust and brief signature of stimulus onset (Gabernet et al. 2005). Feedforward inhibition may serve a similar role in M1–S1 interactions. The prewhisking burst of M1 activity could transiently engage S1 neurons, providing a strong signal of whisking onset; this could set S1 circuits in a state to be further modified by the continued tonic firing of some M1 neurons.

On longer timescales, studies have demonstrated that over the course of a whisking bout the responsiveness of cells in S1 is diminished relative to nonwhisking states (Fanselow and Nicolelis 1999; Hentschke et al. 2006; Ferezou et al. 2007). One possibility is that sustained increases in motor cortex firing during whisking suppress activity in S1. We have demonstrated that such a neural substrate exists in the direct projection from M1 onto S1 inhibitory interneurons. However, given that M1 inputs broadly engage populations of both inhibitory and pyramidal neurons, it seems unlikely that M1 exerts a predominantly inhibitory or excitatory effect on S1. Furthermore, the activity of S1 FS and SOM inhibitory interneurons also decreases during whisking (Gentet et al. 2010, 2012). In the whisker-barrel system, as well as in other somatosensory systems, motor-related gating occurs at subcortical levels (Furuta et al. 2008), resulting in reduced stimulus-evoked thalamic firing (Lee et al. 2008). Therefore, the reduced activity of S1 excitatory and inhibitory neurons during whisking may be a reflection of decreased thalamic input that is not fully compensated for by corticocortical input from M1.

Elevations in motor cortex firing that precede and accompany whisking may produce a barrage of excitatory and inhibitory synaptic activity within S1 that contributes to state-dependent changes observed in cortical neurons during active touch. Transformations in input–output functions of individual pyramidal neurons as well as the correlated activity

between neurons can be regulated dynamically by the timing and rate of excitatory and inhibitory inputs (Chance et al. 2002; Prescott and De Koninck 2003; de la Rocha et al. 2007; Renart et al. 2010). Moreover, M1 inputs are located more distally along S1 apical dendrites than VPm inputs (Petreanu et al. 2009). Changes in the balance of proximal and distal synaptic inputs can also affect neuronal responsiveness (Larkum et al. 2004; Oviedo and Reyes 2005). Whisking-associated reductions in sensory-evoked thalamic activity, accompanied by increases in motor cortex activity, could therefore modify or even sharpen stimulus-encoding properties of S1 neurons. M1 input to S1 inputs may thus contribute to sensorimotor integration by modulating S1 circuits through broad recruitment of both excitatory and inhibitory cell populations.

Funding

This work was supported in part by the National Institute for Neurological Disorders and Stroke (NS19950 to D.J.S.).

Notes

We thank Jason Rampelt for excellent technical assistance and Scott Cruikshank and Barry Connors for valuable advice at critical early stages of this project. We are also grateful to Anne-Marie Oswald and Sashi Marella for suggestions and advice. *Conflict of Interest*: None declared.

References

Agmon A, Connors BW. 1992. Correlation between intrinsic firing patterns and thalamocortical synaptic responses of neurons in mouse barrel cortex. J Neurosci. 12:319–329.

Alloway KD. 2008. Information processing streams in rodent barrel cortex: the differential functions of barrel and septal circuits. Cereb Cortex. 18:979–989.

Alloway KD, Zhang M, Chakrabarti S. 2004. Septal columns in rodent barrel cortex: functional circuits for modulating whisking behavior. J Comp Neurol. 480:299–309.

Ascoli GA, Alonso-Nanclares L, Anderson SA, Barrionuevo G, Benavides-Piccione R, Burkhalter A, Buzsaki G, Cauli B, Defelipe J, Fairen A et al.. 2008. Petilla terminology: nomenclature of features of GABAergic interneurons of the cerebral cortex. Nat Rev Neurosci. 9:557–568.

Beierlein M, Connors BW. 2002. Short-term dynamics of thalamocortical and intracortical synapses onto layer 6 neurons in neocortex. J Neurophysiol. 88:1924–1932.

Beierlein M, Gibson JR, Connors BW. 2003. Two dynamically distinct inhibitory networks in layer 4 of the neocortex. J Neurophysiol. 90:2987–3000.

Boyden ES, Zhang F, Bamberg E, Nagel G, Deisseroth K. 2005. Millisecond-timescale, genetically targeted optical control of neural activity. Nat Neurosci. 8:1263–1268.

Brecht M, Grinevich V, Jin TE, Margrie T, Osten P. 2006. Cellular mechanisms of motor control in the vibrissal system. Pflugers Arch. 453:269–281.

Carvell GE, Miller SA, Simons DJ. 1996. The relationship of vibrissal motor cortex unit activity to whisking in the awake rat. Somatosens Mot Res. 13:115–127.

Cauller LJ, Clancy B, Connors BW. 1998. Backward cortical projections to primary somatosensory cortex in rats extend long horizontal axons in layer I. J Comp Neurol. 390:297–310.

Chance FS, Abbott LF, Reyes AD. 2002. Gain modulation from background synaptic input. Neuron. 35:773–782.

Chapin JK, Woodward DJ. 1982. Somatic sensory transmission to the cortex during movement: gating of single cell responses to touch. Exp Neurol. 78:654–669.

Chmielowska J, Carvell GE, Simons DJ. 1989. Spatial organization of thalamocortical and corticothalamic projection systems in the rat SmI barrel cortex. J Comp Neurol. 285:325–338.

Chung S, Li X, Nelson SB. 2002. Short-term depression at thalamocortical synapses contributes to rapid adaptation of cortical sensory responses in vivo. Neuron. 34:437–446.

Cruikshank SJ, Lewis TJ, Connors BW. 2007. Synaptic basis for intense thalamocortical activation of feedforward inhibitory cells in neocortex. Nat Neurosci. 10:462–468.

Cruikshank SJ, Urabe H, Nurmikko AV, Connors BW. 2010. Pathway-specific feedforward circuits between thalamus and neocortex revealed by selective optical stimulation of axons. Neuron. 65:230–245.

de la Rocha J, Doiron B, Shea-Brown E, Josic K, Reyes A. 2007. Correlation between neural spike trains increases with firing rate. Nature. 448:802–806.

Dittgen T, Nimmerjahn A, Komai S, Licznerski P, Waters J, Margrie TW, Helmchen F, Denk W, Brecht M, Osten P. 2004. Lentivirus-based genetic manipulations of cortical neurons and their optical and electrophysiological monitoring in vivo. Proc Natl Acad Sci USA. 101:18206–18211.

Elhanany E, White EL. 1990. Intrinsic circuitry: synapses involving the local axon collaterals of corticocortical projection neurons in the mouse primary somatosensory cortex. J Comp Neurol. 291:43–54.

Fanselow EE, Nicolelis MA. 1999. Behavioral modulation of tactile responses in the rat somatosensory system. J Neurosci. 19:7603–7616.

Fanselow EE, Richardson KA, Connors BW. 2008. Selective, state-dependent activation of somatostatin-expressing inhibitory interneurons in mouse neocortex. J Neurophysiol. 100:2640–2652.

Fee MS, Mitra PP, Kleinfeld D. 1997. Central versus peripheral determinants of patterned spike activity in rat vibrissa cortex during whisking. J Neurophysiol. 78:1144–1149.

Felleman DJ, Van Essen DC. 1991. Distributed hierarchical processing in the primate cerebral cortex. Cereb Cortex. 1:1–47.

Ferezou I, Haiss F, Gentet LJ, Aronoff R, Weber B, Petersen CC. 2007. Spatiotemporal dynamics of cortical sensorimotor integration in behaving mice. Neuron. 56:907–923.

Friedman WA, Jones LM, Cramer NP, Kwegyir-Afful EE, Zeigler HP, Keller A. 2006. Anticipatory activity of motor cortex in relation to rhythmic whisking. J Neurophysiol. 95:1274–1277.

Friedman WA, Zeigler HP, Keller A. 2012. Vibrissae motor cortex unit activity during whisking. J Neurophysiol. 107:551–563.

Furuta T, Timofeeva E, Nakamura K, Okamoto-Furuta K, Togo M, Kaneko T, Deschenes M. 2008. Inhibitory gating of vibrissal inputs in the brainstem. J Neurosci. 28:1789–1797.

Gabernet L, Jadhav SP, Feldman DE, Carandini M, Scanziani M. 2005. Somatosensory integration controlled by dynamic thalamocortical feed-forward inhibition. Neuron. 48:315–327.

Gentet LJ, Avermann M, Matyas F, Staiger JF, Petersen CC. 2010. Membrane potential dynamics of GABAergic neurons in the barrel cortex of behaving mice. Neuron. 65:422–435.

Gentet LJ, Kremer Y, Taniguchi H, Huang ZJ, Staiger JF, Petersen CH. 2012. Unique functional properties of somatostatin-expressing GABAergic neurons in mouse barrel cortex. Nat Neurosci. advance online publication.

Gil Z, Connors BW, Amitai Y. 1997. Differential regulation of neocortical synapses by neuromodulators and activity. Neuron. 19:679–686.

Gunaydin LA, Yizhar O, Berndt A, Sohal VS, Deisseroth K, Hegemann P. 2010. Ultrafast optogenetic control. Nat Neurosci. 13:387–392.

Hattox AM, Nelson SB. 2007. Layer V neurons in mouse cortex projecting to different targets have distinct physiological properties. J Neurophysiol. 98:3330–3340.

Helmstaedter M, Sakmann B, Feldmeyer D. 2009. L2/3 interneuron groups defined by multiparameter analysis of axonal projection, dendritic geometry, and electrical excitability. Cereb Cortex. 19:951–962.

Hentschke H, Haiss F, Schwarz C. 2006. Central signals rapidly switch tactile processing in rat barrel cortex during whisker movements. Cereb Cortex. 16:1142–1156.
Hill DN, Curtis JC, Moore JD, Kleinfeld D. 2011. Primary motor cortex reports efferent control of vibrissa motion on multiple timescales. Neuron. 72:344–356.
Hooks BM, Hires SA, Zhang YX, Huber D, Petreanu L, Svoboda K, Shepherd GM. 2011. Laminar analysis of excitatory local circuits in vibrissal motor and sensory cortical areas. PLoS Biol. 9:e1000572.
Kapfer C, Glickfeld LL, Atallah BV, Scanziani M. 2007. Supralinear increase of recurrent inhibition during sparse activity in the somatosensory cortex. Nat Neurosci. 10:743–753.
Killackey HP. 1973. Anatomical evidence for cortical subdivisions based on vertically discrete thalamic projections from the ventral posterior nucleus to cortical barrels in the rat. Brain Res. 51:326–331.
Kinnischtzke AK, Sewall AM, Berkepile JM, Fanselow EE. 2012. Postnatal maturation of somatostatin-expressing inhibitory cells in the somatosensory cortex of GIN mice. Front Neural Circuits. 6:33.
Kleinfeld D, Ahissar E, Diamond ME. 2006. Active sensation: insights from the rodent vibrissa sensorimotor system. Curr Opin Neurobiol. 16:435–444.
Krupa DJ, Wiest MC, Shuler MG, Laubach M, Nicolelis MA. 2004. Layer-specific somatosensory cortical activation during active tactile discrimination. Science. 304:1989–1992.
Larkum ME, Senn W, Luscher HR. 2004. Top-down dendritic input increases the gain of layer 5 pyramidal neurons. Cereb Cortex. 14:1059–1070.
Lee S, Carvell GE, Simons DJ. 2008. Motor modulation of afferent somatosensory circuits. Nat Neurosci. 11:1430–1438.
Lee S, Hjerling-Leffler J, Zagha E, Fishell G, Rudy B. 2010. The largest group of superficial neocortical GABAergic interneurons expresses ionotropic serotonin receptors. J Neurosci. 30:16796–16808.
Lee SH, Kwan AC, Zhang S, Phoumthipphavong V, Flannery JG, Masmanidis SC, Taniguchi H, Huang ZJ, Zhang F, Boyden ES et al.. 2012. Activation of specific interneurons improves V1 feature selectivity and visual perception. Nature. 488:379–383.
Ma Y, Hu H, Berrebi AS, Mathers PH, Agmon A. 2006. Distinct subtypes of somatostatin-containing neocortical interneurons revealed in transgenic mice. J Neurosci. 26:5069–5082.
Mao T, Kusefoglu D, Hooks BM, Huber D, Petreanu L, Svoboda K. 2011. Long-range neuronal circuits underlying the interaction between sensory and motor cortex. Neuron. 72:111–123.
Markram H, Toledo-Rodriguez M, Wang Y, Gupta A, Silberberg G, Wu C. 2004. Interneurons of the neocortical inhibitory system. Nat Rev Neurosci. 5:793–807.
Markram H, Wang Y, Tsodyks M. 1998. Differential signaling via the same axon of neocortical pyramidal neurons. Proc Natl Acad Sci USA. 95:5323–5328.
Nagel G, Szellas T, Huhn W, Kateriya S, Adeishvili N, Berthold P, Ollig D, Hegemann P, Bamberg E. 2003. Channelrhodopsin-2, a directly light-gated cation-selective membrane channel. Proc Natl Acad Sci USA. 100:13940–13945.
Nathanson JL, Yanagawa Y, Obata K, Callaway EM. 2009. Preferential labeling of inhibitory and excitatory cortical neurons by endogenous tropism of adeno-associated virus and lentivirus vectors. Neuroscience. 161:441–450.
Oliva AA Jr, Jiang M, Lam T, Smith KL, Swann JW. 2000. Novel hippocampal interneuronal subtypes identified using transgenic mice that express green fluorescent protein in GABAergic interneurons. J Neurosci. 20:3354–3368.
Oswald AM, Doiron B, Rinzel J, Reyes AD. 2009. Spatial profile and differential recruitment of GABAB modulate oscillatory activity in auditory cortex. J Neurosci. 29:10321–10334.
Oswald AM, Reyes AD. 2008. Maturation of intrinsic and synaptic properties of layer 2/3 pyramidal neurons in mouse auditory cortex. J Neurophysiol. 99:2998–3008.
Oswald AM, Reyes AD. 2011. Development of inhibitory timescales in auditory cortex. Cereb Cortex. 21:1351–1361.
Otsuka T, Kawaguchi Y. 2011. Cell diversity and connection specificity between callosal projection neurons in the frontal cortex. J Neurosci. 31:3862–3870.
Oviedo H, Reyes AD. 2005. Variation of input-output properties along the somatodendritic axis of pyramidal neurons. J Neurosci. 25:4985–4995.
Packer AM, Yuste R. 2011. Dense, unspecific connectivity of neocortical parvalbumin-positive interneurons: a canonical microcircuit for inhibition? J Neurosci. 31:13260–13271.
Petreanu L, Mao T, Sternson SM, Svoboda K. 2009. The subcellular organization of neocortical excitatory connections. Nature. 457:1142–1145.
Porter JT, Johnson CK, Agmon A. 2001. Diverse types of interneurons generate thalamus-evoked feedforward inhibition in the mouse barrel cortex. J Neurosci. 21:2699–2710.
Porter LL, White EL. 1983. Afferent and efferent pathways of the vibrissal region of primary motor cortex in the mouse. J Comp Neurol. 214:279–289.
Pouille F, Scanziani M. 2001. Enforcement of temporal fidelity in pyramidal cells by somatic feed-forward inhibition. Science. 293:1159–1163.
Pouille F, Scanziani M. 2004. Routing of spike series by dynamic circuits in the hippocampus. Nature. 429:717–723.
Poulet JF, Petersen CC. 2008. Internal brain state regulates membrane potential synchrony in barrel cortex of behaving mice. Nature. 454:881–885.
Prescott SA, De Koninck Y. 2003. Gain control of firing rate by shunting inhibition: roles of synaptic noise and dendritic saturation. Proc Natl Acad Sci USA. 100:2076–2081.
Renart A, de la Rocha J, Bartho P, Hollender L, Parga N, Reyes A, Harris KD. 2010. The asynchronous state in cortical circuits. Science. 327:587–590.
Reyes A, Lujan R, Rozov A, Burnashev N, Somogyi P, Sakmann B. 1998. Target-cell-specific facilitation and depression in neocortical circuits. Nat Neurosci. 1:279–285.
Rocco-Donovan M, Ramos RL, Giraldo S, Brumberg JC. 2011. Characteristics of synaptic connections between rodent primary somatosensory and motor cortices. Somatosens Mot Res. 28:63–72.
Silberberg G, Markram H. 2007. Disynaptic inhibition between neocortical pyramidal cells mediated by Martinotti cells. Neuron. 53:735–746.
Simons DJ, Carvell GE. 1989. Thalamocortical response transformation in the rat vibrissa/barrel system. J Neurophysiol. 61:311–330.
Swadlow HA. 1989. Efferent neurons and suspected interneurons in S-1 vibrissa cortex of the awake rabbit: receptive fields and axonal properties. J Neurophysiol. 62:288–308.
Swadlow HA. 2003. Fast-spike interneurons and feedforward inhibition in awake sensory neocortex. Cereb Cortex. 13:25–32.
Thomson AM, Lamy C. 2007. Functional maps of neocortical local circuitry. Front Neurosci. 1:19–42.
Veinante P, Deschenes M. 2003. Single-cell study of motor cortex projections to the barrel field in rats. J Comp Neurol. 464:98–103.
White EL, DeAmicis RA. 1977. Afferent and efferent projections of the region in mouse SmL cortex which contains the posteromedial barrel subfield. J Comp Neurol. 175:455–482.
Wilson NR, Runyan CA, Wang FL, Sur M. 2012. Division and subtraction by distinct cortical inhibitory networks in vivo. Nature. 488:343–348.
Wimmer VC, Bruno RM, de Kock CP, Kuner T, Sakmann B. 2010. Dimensions of a projection column and architecture of VPM and POm axons in rat vibrissal cortex. Cereb Cortex. 20: 2265–2276.
Xiang Z, Huguenard JR, Prince DA. 2002. Synaptic inhibition of pyramidal cells evoked by different interneuronal subtypes in layer v of rat visual cortex. J Neurophysiol. 88:740–750.
Zhang ZW, Deschenes M. 1997. Intracortical axonal projections of lamina VI cells of the primary somatosensory cortex in the rat: a single-cell labeling study. J Neurosci. 17:6365–6379.